Low-order models of a single-screw expander for organic Rankine cycle applications

2015 IOP Conf. Ser.: Mater. Sci. Eng. 90 012061

(http://iopscience.iop.org/1757-899X/90/1/012061)

Low-order models of a single-screw expander for organic Rankine cycle applications

D. Ziviani[1], A. Desideri[2], V. Lemort[2], M. De Paepe[1], M. van den Broek[1]

[1]Department of Flow Heat and Combustion Mechanics - Ghent University - UGent, Sint-Pietersnieuwstraat 41, 9000 Gent, Belgium
[2]Aerospace and Mechanical Engineering Department, University of Liège, Campus du Sart Tilman B49, B-4000 Liège, Belgium

E-mail: davide.ziviani@ugent.be,adesideri@ulg.ac.be, martijn.vandenbroek@ugent.be, michel.depaepe@ugent.be, vincent.lemort@ulg.ac.be

Abstract. Screw-type volumetric expanders have been demonstrated to be a suitable technology for organic Rankine cycle (ORC) systems because of higher overall effectiveness and good part-load behaviour over other positive displacement machines. An 11 kWe single-screw expander (SSE) adapted from an air compressor has been tested in an ORC test-rig operating with R245fa as working fluid. A total of 60 steady-steady points have been obtained at four different rotational speeds of the expander in the range between 2000 rpm and 3300 rpm. The maximum electrical power output and overall isentropic effectiveness measured were 7.3 kW and 51.9%, respectively. In this paper, a comparison between two low-order models is proposed in terms of accuracy of the predictions, the robustness of the model and the computational time. The first model is the Pacejka equation-based model and the second is a semi-empirical model derived from a well-known scroll expander model and modified to include the geometric aspects of a single screw expander. The models have been calibrated with the available steady-state measurement points by identifying the proper parameters.

1. Introduction

A combination of concern for the environment, current energy policies, and favorable economics continues to push energy research in two key areas: further development of alternative energy sources and better utilization of traditional energy sources. With reference to the latter, waste heat recovery is gaining attention and organic Rankine cycle (ORC) technology has been widely demonstrated to be viable to harness low-grade heat sources. The operating principle is based on exploiting the thermal energy from the heat source by means of an evaporator and producing electricity by reducing the high-enthalpy content working fluid through an expander coupled with an electric generator. Besides turbines [1] which often are too expensive even though they present high efficiency, researchers are focusing on finding suitable expansion devices for different applications and power ranges. Furthermore, especially in the low power range, dynamic expanders become less cost-effective. The production of useful work from an ORC relies on the expander behavior and especially at lower capacity range it is challenging to find a device with efficient performance. Volumetric type expanders have been suggested by several authors as a suitable

Nomenclature

A	Area (m^2)
AU	Overall heat transfer conductance (kW/K)
D	Diameter (m)
h	Specific enthalpy (kJ/kg)
i	Transmission Ratio (-)
L	Length (m)
m	Mass (kg)
$\dot{m}$	Mass flow rate (kg/s)
N	Rotational speed (-)
p	Pressure (kPa)
$\dot{Q}$	Heat rate (kW)
r_v	Volume ratio (-)
r_p	pressure ratio (-)
T	Temperature (K)
u	Uncertainty (-)
v	Specific volume (m^3/kg)
V	Volume (m^3)
$\dot{V}$	Volumetric flow rate (m^3/s)
w	Specific work (kJ/kg)
$\dot{W}$	Power (W)
z	Number of grooves or teeth (-)
ϕ_{FF}	Filling factor (-)
ε	Effectiveness (-)
η	Efficiency (-)

Subscript

amb	ambient
crit	critic
ex	exhaust
exp	expander
el	electric
d	discharge
eff	effective
g	groove
int	internal
is	isentropic
l	liquid
m	mechanical
meas	measured
nom	nominal
oa	over-all
pp	pump
su	supply
sh	shaft
sr	screw rotor
sw	starwheel
r	refrigerant
ref	reference
th	theoretical
v	volume

solution because of their higher expansion ratio and higher efficiency in the small scale and their tolerance to two-phase flow conditions. In many cases, the volumetric expanders are obtained by reversing and optimizing the corresponding compressors available on the market, e.g. scroll-type [2]. Among them, screw-type expanders are characterized by large volume ratios (from 2 to 5.3) and isentropic efficiency up to 85% [3]. In this paper, the performance of a single-screw expander is characterized by two low-order models based on experimental data obtained from an 11 kWe ORC running with R245fa. Insights on a deterministic model of the same machine are presented in a companion paper [4].

2. Single-screw expander and ORC test rig

In the present study, a single-screw expander (SSE) is considered. The SSE is based on the meshing between a grooved central rotor with two toothed gaterotors (or starwheels), as shown in Fig. 1(a). In particular, the rotor has 6 grooves and each of the starwheel disks have 11 teeth. The meshing isolates a flute on each side of the rotor leading to a symmetrical expansion process with respect the rotation axis of the rotor. As a consequence, the machine is characterized by balanced loading, low vibrations and long service life. The SSE tested, shown in Fig.1(a), is an adapted oil-injected air-compressors coupled with a 11 kWe asynchronous generator and the main geometric parameters are listed in Tab. 1. The SSE is installed in a small-scale industrial-based ORC. The layout of the system and the location of the sensors are illustrated in Fig.1(b). The experimental setup includes a 14-stage centrifugal pump with a maximum operating pressure of 14 bar and 2.2 kWe nominal power, three identical brazed plate heat exchangers, acting as evaporator, condenser and internal heat exchanger and a liquid receiver. Additional information regarding the installation can be found in [5]. The pump motor and

Table 1. Geometric parameters of single-screw expander.

i	[-]	11/6
D_{sr}	[mm]	122
$V_{g,max}$	[cm^3]	57.39
$r_{v,built-in}$	[-]	4.7
w	[m]	18.5
L_{rotor}	[m]	121

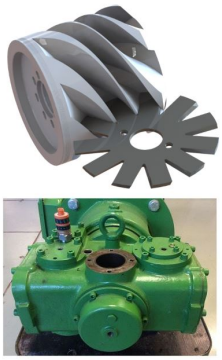

(a)

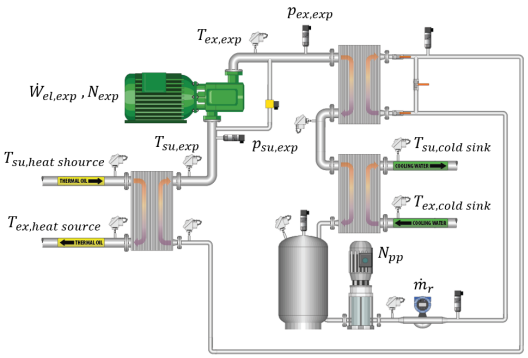

(b)

Figure 1. (*a*) 3D CAD view of the meshing of the main rotor and the gaterotor of a single-screw expander (top); picture of the single-screw expander installed in the ORC system (bottom); (*b*) schematic of the ORC installation.

Table 2. Minimum and maximum values of the measured and derived variables.

	Measured independent variables			Measured dependent variables				Performance indicators	
	$p_{su,exp}$ (kPa)	$p_{ex,exp}$ (kPa)	$T_{su,exp}$ (°C)	ΔT_{sh} (K)	$\dot{m}$ (kg/s)	$\dot{W}_{el,exp}$ (W)	$T_{ex,exp}$ (°C)	$\varepsilon_{is,oa,exp}$ (-)	ϕ_{FF} (-)
Min	566	120	106.7	26	0.12	1283	75.5	0.2058	1.038
Max	1230	232	124.9	50	0.37	7364	104.6	0.5191	1.331

the expander electrical generator are controlled by two inverters. The working fluid selected is R245fa, which replaces the SES36 previously investigated by the authors [5]. The refrigerant is mixed with approximately 3% vol. of lubricant oil and a bleeding line after the pump ensures the lubrication of the expander. Thermodynamic calculations are performed in real time with the CoolProp wrapper for LabView [6].

3. Experimental data discussion

A total of 60 steady-state points have been determined from the experimental data. The maximum and minimum values of the measured and calculated variables are listed in Tab. 2. The tests have been performed by maintaining fixed the thermal oil supply temperature at 125°C as well as the cooling loop flow rate (water + 30% vol. glycol) at 4.166 kg/s. The mass flow rate of the working fluid has been controlled by setting the pump frequency between 25 Hz and 40 Hz. Four different rotational speeds of the expander have been considered, i.e. 2000 rpm, 2500 rpm, 3000 rpm, 3300 rpm. For all the collected measurements the fluid was entering the expander in vapor phase/ superheated condition. Due to the fact that the cold sink relies on the external conditions (air cooled loop), the condensing temperature and pressure of the ORC were not constant. This situation is shown in Fig. 2(a) where the power output is plotted as a function of the condensing pressure with a contour representing the condensing temperature. The tests have been carried out by considering two rotational speeds in each testing day and the measured points are clearly grouped. The external temperature was varying not only during the daytime, as normally occurs, but also different weather conditions have been encountered in different days. By analyzing Fig. 2(a), it is clear that the data are influenced by the air-cooled condenser. The test conducted at 2000 rpm and 3000 rpm will be considered as a reference,

although the models will be validated by considering all the rotational speeds. In Fig. 2(b), the data shows the range of electric power out and pressure ratios reached during the testing. Generally, the performance of a positive-displacement expander can be expressed in terms of isentropic efficiency and volumetric efficiency. The latter is normally defined by the filling factor which can assume values greater than one for an expander. The adiabatic definition of the isentropic efficiency cannot be directly applied in the case of volumetric expander [2]. Mathematically, the filling factor is given by:

$$\phi_{FF} = \frac{\dot{m}_{meas} v_{su,exp}}{\dot{V}_{swept,th}} = \frac{\dot{m}_{meas} v_{su,exp}}{2\, z_{sr}\, V_{g,su}\ (N_{rot,exp}/60)} \tag{1}$$

where the volume of the groove at suction closure, $V_{g,su}$, is determined by the geometric model described in details in the companion paper [4]. Because of the absence of a torque meter installed at the expander shaft and temperature measurements on the expander shell, an overall isentropic effectiveness of the expander and generator is adopted by relating the measured electrical power output at the inverter and the isentropic expansion power, i.e.:

$$\varepsilon_{is,oa,meas} = \frac{\dot{W}_{el,meas}}{\dot{W}_{is,exp}} = \frac{\dot{W}_{el,meas}}{\dot{m}_{meas}\,(h_{su,exp} - h_{ex,is,exp})} \tag{2}$$

At the nominal speed of 3000 rpm, the maximum electrical power output and overall isentropic effectiveness achieved were 7364 W and 51.91%, respectively. Additional considerations can be done on the volumetric performance of the machine. In fact, in Fig. 2(c), the filling factor (1) at different rotational speeds is plotted as function of the expander inlet pressure. It becomes clear that the filling factor of this machine mainly depends on the rotational speed and it is less sensitive to the supply pressure variations. In particular, the higher the rotational speed the closer the filling factor reaches unity, meaning the leakages are reduced. Thus, since 3000 rpm is the nominal speed, the contour shows the maximum overall isentropic effectiveness around $\phi_{FF} \cong 1.05$. After the tests, an inspection has been conducted to assess the status of the expander. The tooth flank sealing profiles were worn out, which could have played a major role in the leakage. This fact may partially explain the value of the filling factor greater than one. Additional issues have been identified for the lubrication systems. In fact, most of the orifices that ensure the injection of the oil, were occluded. Most likely, the expander was running without proper lubricant injection for several working hours, affecting negatively the performance. The only oil entering the expander was the amount in solution with the refrigerant. This fact may explain large leakages at lower rotational speeds, i.e. higher values of the filling factor. Due to the variability of the test conditions, the overall isentropic effectiveness exhibits different trends by varying the rotational speed which it makes difficult to draw general conclusions on the performance of the machine, as shown in Fig. 2(d). However, it is possible to notice that the overall isentropic effectiveness increases with the increase of the pressure ratio until the internal limit of the SSE is reached, i.e. fixed built-in volume ratio. At higher pressure ratios, the power output still increases, but the overall isentropic effectiveness is penalized. The measurements for rotational speeds 2500 rpm and 3300 rpm do not provide any further information. These data points present a similar trend to 2000 rpm and 3000 rpm at least between pressure ratio, $r_{p,exp}$, 3 and 4. Additionally, by adopting the correlations obtained by [7] for the inverter electrical effectiveness and the generator efficiency, the expander isentropic efficiency at the shaft, $\eta_{is,sh}$, has been estimated and included in Fig. 2(d).

4. Low-order models

The characterization of a volumetric expander is based on a set of typical parameters such as pressure ratio, actual volume ratio and rotational speed as well as performance indexes, typically

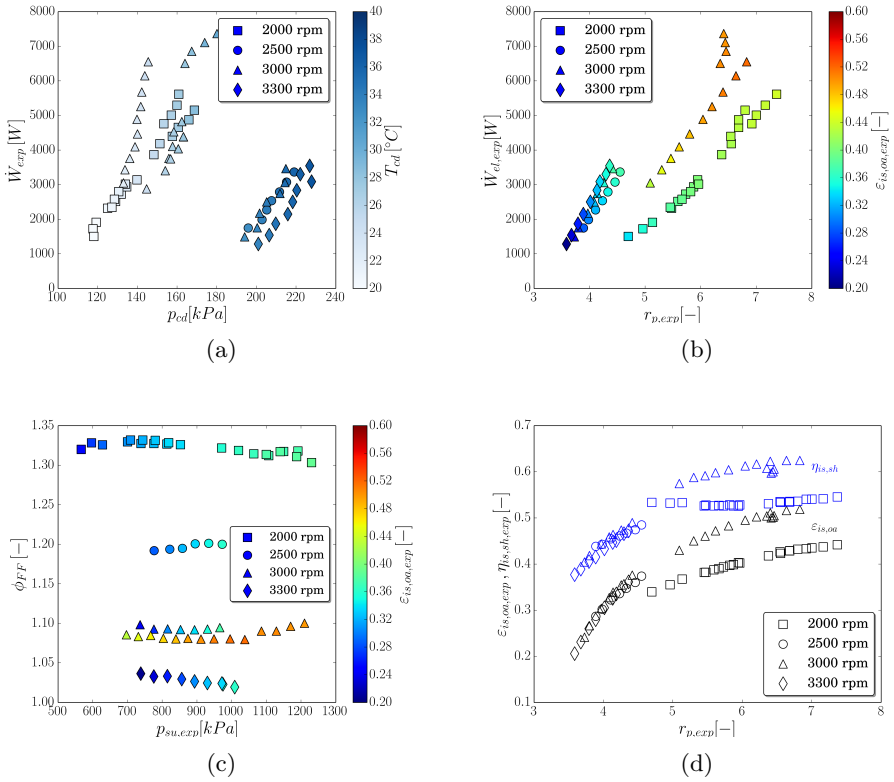

Figure 2. (a) Influence of the condensing temperature and pressure on the electrical power output due to the air condenser;(b) plot of the expander electrical power output as function or the pressure ratio at different rotational of the 60 steady-state points obtained. The contour is representative of the overall isentropic effectiveness ; (c) influence of the supply pressure of the expander on the filling factor; (d)Overall isentropic effectiveness, $\varepsilon_{is,oa}$, and isentropic efficiency, $\varepsilon_{is,sh}$, at the shaft as a function of pressure ratio at different rotational speed.

isentropic efficiency and filling factor. Empirical and semi-empirical models, usually referred as low-order models, are useful to describe the behavior of the expander with low computational effort with respect to more detailed models. Furthermore, these types of models can be easily integrated in cycle simulations to evaluate the impact of the expander behavior at full or part-load conditions. In this paper, two methodologies are proposed to describe the performance of the single screw expander. It should also be noted that the analyses and considerations within this paper are valid for R245fa. Desideri et al. [8] analyzed the same expander by using SES36 as working fluid.

4.1. Pressure ratio based equation

The inlet pressure, $p_{su,exp}$, the pressure ratio over the expander, r_p, and the rotational speed, $N_{rot,exp}$, are the three working condition variables selected to represent the expander behavior. In this paper, a similar nomenclature has been adopted. The aforementioned variables are expressed in terms of non-dimensional form by considering a set of reference conditions:

$$r_p^* = \frac{r_p - r_{p,ref}}{r_{p,ref}} \; ; N_{exp}^* = \frac{N_{exp} - N_{exp,ref}}{N_{exp,ref}} \; ; p^* = \frac{p_{su,exp} - p_{su,exp,ref}}{p_{su,exp,ref}} \tag{3}$$

where $r_{p,ref} = 6$, $N_{exp,ref} = 3000$ and $p_{su,exp,ref} = 10$. A generic non-dimensional expression similar to Pacejka's equation is used to calculate the overall isentropic effectiveness as a function of the previously defined variables and additional parameters. The complete mathematical formulation can be found in [2].

4.2. Semi-empirical model

The semi-empirical model adopted is based on the model described by Lemort et al. [9] which retains the main physical aspects of the expansion device. The entire expansion process from suction to discharge is decomposed into a number of consecutive steps: an adiabatic supply pressure drop, an isobaric supply cooling-down, an isentropic expansion to the pressure imposed by the built-in volume ratio of the expander, an adiabatic expansion at a constant machine volume, an adiabatic mixing between supply and leakage flows and an isobaric exhaust cooling-down or heating-up. The model estimates the discharge temperature, the mass flow rate, the overall isentropic effectiveness, the expander work and power losses. Due to the fact that the model was tailored mainly on scroll-type machines, an extension is proposed hereafter to include the particular features of a SSE. A graphical representation of the model is shown in Fig. 3. The expansion process in the SSE occurs simultaneously on both sides of the rotor and the two parts are not in communication unless unforeseen leakages occur. Therefore, the inlet flow (su) enters the expander and it is subject to a pressure loss ($su \rightarrow su_{in}$) due to the suction port, modeled with a converging-diverging nozzle characterized by a throat cross-section, $A_{c,su}$. The total mass flow rate entering the expander, $\dot{m}_r$, splits to reach the two suction ports, $\dot{m}_r = \dot{m}_r^{'} + \dot{m}_r^{''}$. Theoretically, the mass flow is equally distributed inside the expander. However, a slight pressure difference may occur due to the difference in shape and length of the internal channels in the housing of the expander. Two lumped pressure drops account for the internal dimension of the channels ($su_{in,1}^{'} \rightarrow su_{in,2}^{''}$). Heat losses during the supply process are considered by defining a fictitious isothermal wall representing the metallic housing of the expander with associated temperature T_{wall}. The cooling down due to temperature difference between working fluid and the wall is modeled by the ε-NTU method characterized by an overall heat transfer $AU_{su}^{'}$ [9] and the total heat loss $\dot{Q}_{su}$ is the sum of the two contributions $\dot{Q}_{su} = \dot{Q}_{su}^{'} + \dot{Q}_{su}^{''}$ In a single-screw machine 9 leakage paths can be distinguished [10]. In this model, the leakages are lumped together by considering an equivalent isentropic flow of a perfect gas through a simply convergent nozzle, where the throat pressure is limited by choked flow conditions. The nozzle is characterized by a fictitious area A_{leak} [9]. Since the leakage model depends on the current pressure and temperature conditions, each side of the rotor may have different values of the leakage cross-section area. The expansion process is divided in two steps accounting for an adiabatic and reversible expansion, $w_{int,s=const}^{'}$, followed by an adiabatic expansion at constant volume,$w_{int,v=const}^{'}$. The work associated with both steps can be expressed by:

$$\dot{W}_{int}^{'} = \dot{m}_{r,in}^{'} \left[h_{r,su2}^{'} \left(p_{r,su2}^{'}, T_{r,su2}^{'} \right) - h_{r,int}^{'} \left(s_{r,int}^{'}, v_{r,int}^{'} \right) + v_{r,int}^{'} \left(p_{r,int}^{'} - p_{r,ex2}^{'} \right) \right] \quad (4)$$

The expanding working fluid on both sides of the rotor contributes to generate mechanical work through the shaft, i.e. $\dot{W}_{int} = \dot{W}_{int}^{'} + \dot{W}_{int}^{''}$. Therefore, the mechanical losses due to friction between the starwheel teeth and the rotor as well as in the bearings can be lumped to a fictitious torque, τ_{loss}, and a term proportional to $\dot{W}_{int}$:

$$\dot{W}_{loss} = \dot{W}_{loss,0} + 2\,\pi\,\tau_{loss}\,\frac{N_{exp}}{60} \quad (5)$$

Once the expansion process is completed, the internal refrigerant flow is mixed with the leakage flow. An additional mixing occurs prior discharge between the flows from each side of the rotor.

The exhaust heat transfer, $\dot{Q}_{ex}$, and the outlet pressure drop are derived similarly as on the supply ones [9]. To be noted is that the inlet pressure drops have a key role in the case of an expander. Finally, an overall energy balance with the fictitious isothermal wall is minimized by the solver to guarantee convergence of the model:

$$\begin{aligned} \dot{W}_{loss} + \dot{Q}_{su} - \dot{Q}_{ex} - \dot{Q}_{amb} = 0 \\ \dot{Q}_{amb} = AU_{amb}\,(T_{wall} - T_{amb}) \end{aligned} \tag{6}$$

Given the supply conditions and the discharge pressure, a set of parameters have to be identified in order to run the model. The model inputs and outputs a well as the set of parameters are listed in Fig. 3.

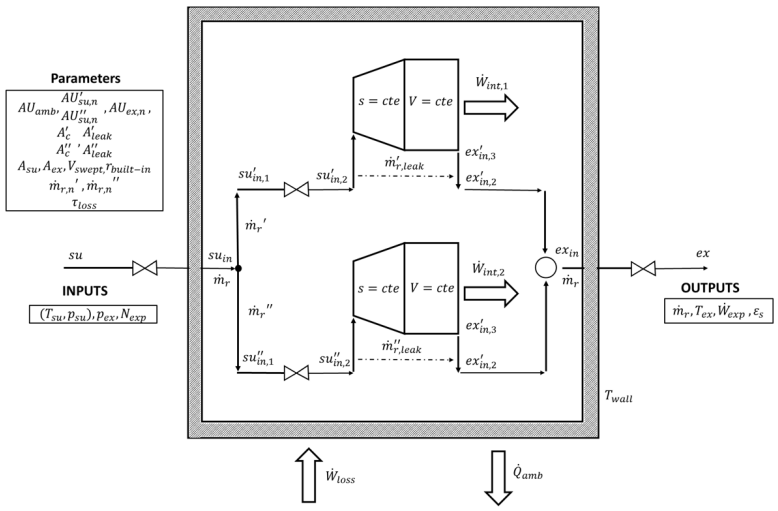

Table 3. Identified parameters of the semi-empirical model.

Parameter	Unit	Value
AU_{amb}	W/K	8.63
$AU'_{su,n}$	W/K	11.75
$AU''_{su,n}$	W/K	13.75
$AU_{ex,n}$	W/K	6.44
$\dot{m}'_{r,n}$	kg/s	0.21
$\dot{m}''_{r,n}$	kg/s	0.27
A'_{leak}	m^2	4.61e-6
A''_{leak}	m^2	6.61e-6
A_{su}	m^2	8.36e-5
A_{ex}	m^2	1.45e-3
α_{loss}	-	0.28
τ_{loss}	Nm	1.25
$\dot{W}_{loss,0}$	W	60.8

Figure 3. Semi-empirical model of the single screw expander.

5. Parameters identification

The two models described include a number of parameters that have to be identified in order to accurately predict the performance of the SSE. The set steady-state points are used to calibrate the models. The empirical parameters, $\mathbf{p} = (a_0, ..., a_6)$ of the Pacejka equation [2] are obtained by minimizing an objective function defined as the sum of the quadratic deviation of the measured and calculated values of the overall isentropic effectiveness scaled by the data uncertainties :

$$r_{Pacejka} = \sum_i \frac{\left(\varepsilon_{is,oa,exp,meas,i} - \varepsilon_{is,oa,exp,calc,i}(\mathbf{p})\right)^2}{u_i^2} \tag{7}$$

Since the the overall isentropic effectiveness measured values, shown in Fig. 2(d), have not a unique trend, a constrained Sequential Least SQuares Programming (SLSQP) minimization algorithm is used to drive to zero the objective function. In particular, the parameters which have physical meaning, i.e. $r_{p,0,nom}$, $r_{p,max,nom}$, $\varepsilon_{is,oa,max}$, $\left(d\varepsilon_{is,oa,max}/dr_{p,0}\right)_{nom}$, $N_{exp,nom}$, have been determined in accordance to [2]. Instead, for the empirical parameters $a_0, ..., a_6$ and ξ a set of boundaries have been determined.

Table 4. Identified Pacejka equation parameters.

Parameter	Value	Empirical parameters:
$r_{p,0,nom}$	3.07600000e+0	a_0 =-1.93529023e-3
$r_{p,max,nom}$	5.99558088e+0	a_1 =-1.25256170e-2
$\varepsilon_{is,oa,max}$	5.19000000e-1	a_2 =-1.17292542e-1
$(d\varepsilon_{is,oa,max}/dr_{p,0})_{nom}$	7.08651674e-1	a_3 =-4.73874764e-2
ξ	1.23877317e+0	a_4 =7.80410436e+0
$N_{exp,nom}$	3.54700000e+3	a_5 =6.36530295e-4
		a_6 =5.78187315e-1

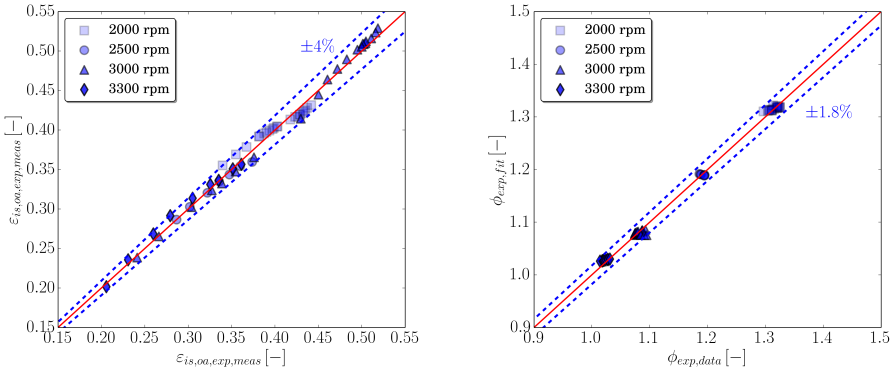

(a) (b)

Figure 4. (a) Comparison between Pacejka-based model and experimental data in terms of parity plot between measured and calculated overall isentropic effectiveness; (a) parity plot of the filling factor.

The semi-empirical model of the SSE presents a higher level of complexity in terms of number of equations to be solved and related numerical issues. Thus, 9 parameters have to be identified by minimizing an object function based on the experimental data. The objective function represents a cumulative error of the three main variables considered in the calibration process, i.e. mass flow rate, discharge temperature and power output. Its expression is given by:

$$r_{SemiEmp} = \sqrt{\sum_i \left(\frac{\dot{m}_{r,i} - \dot{m}_{r,meas,i}}{\dot{m}_{r,meas,i}}\right)^2} + \sqrt{\sum_i \left(\frac{\dot{W}_{exp,i} - \dot{W}_{exp,meas,i}}{\dot{W}_{exp,meas,i}}\right)^2} + \sqrt{\sum_i \left(\frac{T_{r,ex,,i} - T_{r,ex,meas,i}}{T_{r,ex,meas,max} - T_{r,ex,meas,min}}\right)^2} \tag{8}$$

To be noted that the term accounting for the difference between measured and calculated discharge temperature has been given a higher weight. The parameter identification is done by using a genetic algorithm with proper bounds for each of the parameters listed in Tab. 3.

6. Results and discussion

The described models have been implemented in the Python language. The minimization process of the objective function for the Pacejka equation requires a limited computational effort to converge. However, the bounds of the SLSQP should be refined a few times in order to achieve the best fit. The set of identified parameters are listed in Tab. 4. By considering all the rotational speeds, i.e. 2000 rpm, 2500 rpm, 3000 rpm and 3300 rpm, a coefficient of determination, R^2, of 99.32% is obtained for the overall isentropic effectiveness with a maximum relative error of 4.05%, as shown in Fig. 4(a). If only the rotational speeds of 2000 rpm and 3000 rpm are

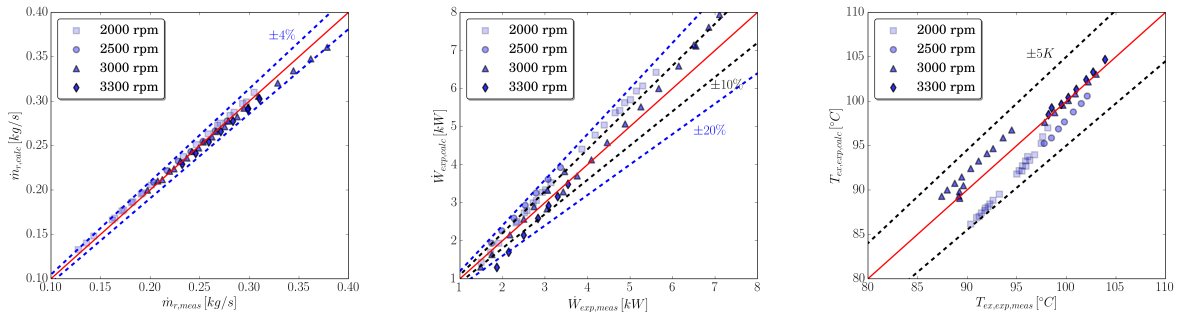

(a) (b) (c)

Figure 5. Parity plots with the optimized parameters: (a) mass flow rate; (b) power output; (c) discharge temperature.

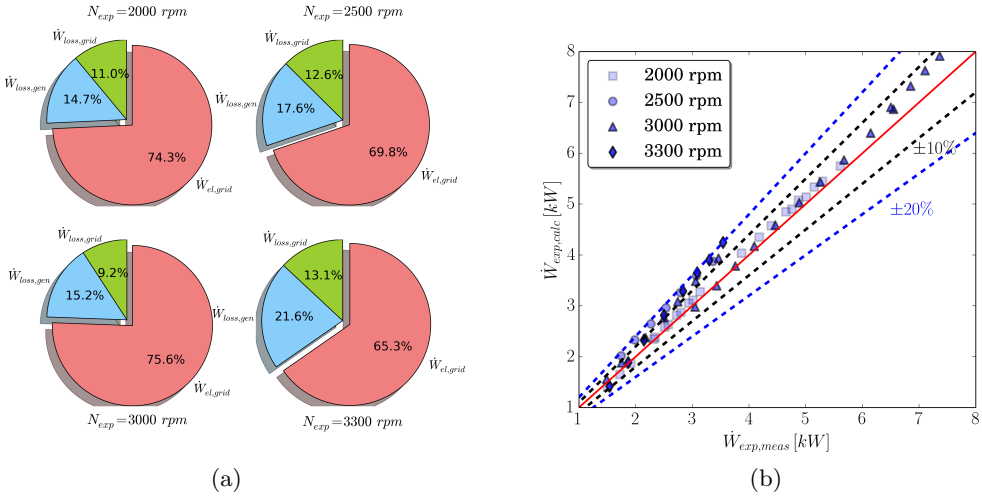

(a) (b)

Figure 6. (a) Distribution of the electro-mechanical losses associated with the coupling of the expander shaft to the generator and inverter, at different rotational speed; (b) improved agreement of the electrical power output by integrating specific correlations of for generator and inverter losses.

considered because investigated during the same day of testing and throughout a wider range of conditions, the R^2 increases slightly to 99.69% and the relative error is reduced by the 30%. The filling factor data points are fitted with R^2 of 99.71% and a maximum relative error of 1.76%, as shown in Fig. 4(b).

The search of the optimized parameters is more involved and lengthy for the semi-empirical model. Although the total number of parameters of the models is comparable, the solution process of the semi-empirical model includes more iterative loops, especially for the calculation of the flow through fictitious nozzles and heat transfer, and, moreover, the parameters are coupled because it is a physical-based model. The optimization process starts by considering only the nominal speed at 3000 rpm in order to obtain a better set of guess parameters. Then, all the data points are considered in the optimization and the genetic algorithm keeps evolving by selecting new generations of parameters based on a natural selection process. The time required to obtain the optimized parameters varies a lot, depending on the selected tolerance of the converging criteria. Reasonable maximum relative errors between measured and calculated

values of mass flow rate, power output and discharge temperature have been selected as the upper limit of the results presented in [9]. In particular, the optimization process has been considered successful if the maximum relative errors between measured and estimated values were 5%, 10% and 5 K for the mass flow rate, power output and discharge temperature, respectively. The optimized parameters are listed in Tab. 3. The parity plots are shown in Fig 5. As a result, the semi-empirical model was able to capture the trend of the experimental data. The mass flow rate is estimated within 4% at all the rotational speeds which means that the geometric parameters and the leakage model have been able to match the real behavior of the machine, as shown in Fig. 5(a). The discharge temperature is predicted within 3 K only at 2500 rpm, 3000 rpm and 3300 rpm. At 2000 rpm, the discharge temperature is underestimated in the range of 3 K up to 5 K, as shown in Fig. 5(c). There is a certain dependency of the heat transfer rate with the rotational speed and therefore the current correlation used should be further modified. Finally, the power output has been predicted within 10% only at the nominal speed of 3000 rpm and few points at 3300 rpm. The power output is generally overestimated at all the other rotational speeds, i.e. 2000 rpm and 2500 rpm. The parity plots presented in Fig. 5 have been obtained by considering the mechanical losses to vary linearly with a mechanical loss torque as shown in Eq. 5. An additional term proportional to the rotational speed similar to the one proposed in [11] was also added to account for the electrical losses from the generator and inverter. By observing Fig. 5(b), it is clear that a different model has to be used to better describe the mechanical losses especially at lower speeds. Furthermore, in the optimization process, the value of the generator efficiency and inverter effectiveness should be considered. Therefore, the performance maps of generator and inverter have been included in the semi-empirical model in order to better estimate the shaft power. The efficiency of the generator depends on the torque and rotational speed, instead the effectiveness of the inverter is mainly related to the electrical power [7]. In Fig. 6(a), a comparison between the actual electrical power output and the electro-mechanical losses for each rotational speed is proposed. Two general considerations can be made related to the uncertainties of the semi-empirical model on the predictions of the electrical power output. First of all, the electrical losses of the inverter are almost constant throughout the power range investigate except at below 2000 W, where they decreases sharply [7]. Secondly, the mechanical efficiency of the generator is strongly related to the rotational speed and the torque applied. At low rotational speed and low torque the efficiency decreases significantly [7]. These behaviors can be found in Fig. 6(a). By recalling that for the rotational speeds of 2500 rpm and 3300 rpm, low values of the power output were achieved, the mechanical efficiency of the generator accounts for 17.6% and 21% of the total shaft power, respectively. The mechanical loss term have been modified with an additional contribution proportional to the internal power, i.e. $\alpha_{loss}\dot{W}_{in}$. As a result, the electrical power output has been predicted within 10% for all the experimental points, as shown in Fig. 6(b). Mass flow rate and discharge temperature predictions slightly improved and the maximum relative errors have been reduced to 3.5% and 4 K,respectively. To be noted is that if only the nominal rotational speed is considered, the mass flow rate, the power output and the discharge temperature are predicted within $\pm 3\%$, $+7\%$ and $+3$ K respectively. It is important to mention that semi-empirical models such as those one proposed in this paper, are calibrated and optimized for a particular machine and for a range of operating conditions. Extrapolating results to larger/smaller machines may result in large errors. For this reason, a larger single-screw expander will be tested and the model extended to include the scale effects and generalize the model from a single machine to a class of machines. The computational time of a single run of the semi-empirical model is around 2.5 seconds. Instead the validation for the all 60 steady-state points takes around 97 seconds. As a comparison, the fastest simulation of the corresponding deterministic model takes approximately 30 seconds.

7. Conclusions

In his paper, the experimental data of a 122 mm single-screw expander for organic Rankine cycle applications have been discussed and further used to calibrate two low-order models, for instance the Pacejka equation for the overall isentropic effectiveness and a semi-empirical model based on the physical aspects of the expander. From the experimental data, the maximum power output obtained was 7.364 kW and a maximum overall isentropic effectiveness of 51.91% was achieved. The calibration of the Pacejka equation resulted in a maximum relative error of 4.05%. By means of a genetic algorithm, the parameters of the semi-empirical model have been determined and the model was able to capture the physical behavior of the SSE. Mass flow rate, power output and discharge temperature have been initially predicted within 5%, 10% and 5 K, respectively for most of the experimental points. A better characterization of the electro-mechanical losses to account for the generator and the inverter has been successively included which led to improved agreement between the measured and calculated values. The maximum isentropic efficiency obtained at the shaft was around 62%.

Acknowledgment

The authors would like to thank graduate student Nelson James from the Herrick Laboratories, Purdue University for his contribution related to the implementation of the genetic algorithm used in this paper.

References

[1] Uusitalo A, Turunen-Saaresti T, Honkatukia J, Colonna P and Larjola J 2013 *J. Eng. Gas Turbines and Power* **135** 1–9

[2] Declaye S, Quoilin S, Guillaume L and Lemort V 2013 *Energy* **55** 173–183

[3] Avadhanula V K and Lin C S 2014 *J. Eng. Gas Turbine and Power* **136** 1–8

[4] Ziviani D, Bell I, Paepe M D and van den Broek M 2015 Update on single-screw expander geometry model integrated into an open-source simulation tool *9th Int. Conf. on Compressors and their Systems, City University of London, London* 39

[5] Gusev S, Ziviani D, Bell I and M De Paepe M v d B 2014 Experimental comparison of working fluids for organic rankine cycle with single-screw expander *Proceedings of 15th Int. Refrig. Air Cond. Conf. at Purdue* 2653

[6] Bell I H, Wronski J, Quoilin S and V L 2014 *Ind. Eng. Chem. Res.* **53** 2498–2508

[7] Melotte N 2012 *Experimental study and dynamic modeling of a Waste Heat Recovery Organic Eankine Cycle* Master's thesis University of Liege

[8] Desideri A, van den Broek M, Gusev S, Lemort V and Quoilin S 2014 Experimental campaign and modeling of a low-capacity waste heat recovery system based on a single screw expander *Proceedings of 22nd Int. Compr. Eng. Conf. at Purdue* 1451

[9] Lemort V, Quoilin S, Cuevas C and Lebrun J 2009 *Applied Thermal Engineering* **29** 3094–3102

[10] Ziviani D, Bell I, De Paepe M and van den Broek M 2014 Comprehensive model of a single screw expander for orc-systems applications *22th Int.Compressor Engineering Conf. at Purdue* 1506

[11] Lemort V, Declaye S and Quoilin S 2011 *Proc. IMechE, Part A: J. Power and Energy* **226** 126–136